IMPACT BASIN FORMATION: THE MANTLE EXCAVATION PARADOX RESOLVED. S. T. Stewart. Department of Earth & Planetary Sciences, Harvard University, Cambridge, MA, USA (sstewart@eps.harvard.edu)

Introduction. The scaling laws for impact crater excavation [1] predict the ejection of mantle material for basin-sized craters (e.g., >100 km on the Moon [2]). However, mantle materials are generally not observed in and around impact basins [3]. Only last year, the spectroscopic detection of olivine in sparse concentric rings around several lunar impact basins was proposed to have a mantle origin [4]. Previous numerical simulations of impact basin formation all suggest significant exposure of mantle material within a central melt pool and in ejecta overlying the overturned crust [5-10]. The scaling laws for transient crater size and depth of excavation are well tested [5, 11-13]. Hence, the paradox is the simultaneous excavation of the mantle with very limited exposure of mantle materials at the end of basin formation.

The paradox is resolved by new insight into (i) the rheology of the mantle during the collapse of the transient cavity and (ii) the extent of removal of crustal materials from the central melt pool. New numerical simulations indicate that the final impact basin would contain discontinuous patches of mantle materials in the terrace zone of an impact basin. These results are in agreement with spatial distribution of olivine observed in impact basins on the Moon [4] and Mars [14, 15].

Numerical Model. Basin formation is modeled using the CTH shock physics code [16] with a fixed central gravity field in 2D and self-gravity in 3D. Planets are initialized in gravitational equilibrium with thermal profiles appropriate for the early Solar System [17, 18]. Multiphase model equations of state are used for iron [19], forsterite [20], and silica [21]. The pressure, temperature, and strain-rate dependent rheological model includes a brittle regime for the crust and uppermost mantle [22, 23] and a creep regime for the deeper mantle [24]. The peridotite solidus and olivine liquidus are used to calculate melting [25]. All model parameters are constrained by laboratory data.

Mantle rheology. In previous numerical simulations, materials heated to and above the solidus were essentially modeled as strengthless fluids. It has long been recognized that the depth of shock-induced melting exceeds the excavation depth in basin forming events [26]. Thus, the collapse of the transient cavity involves significant amounts of melted material. As a result, the gravitationally-driven collapse of the transient crater led to significant overshoot and sloshing of mantle materials onto the surrounding crust [5-10].

In this work, it is recognized that the collapse of the mantle involves a two-phase flow of melt and solid clasts. Under the high strain rates of crater collapse, the ratio of clast inertia to viscous forces (the Bagnold number) is high; as a result, the shear stresses are determined by collisions between the solid clasts [27]. Furthermore, the convergent geometry ensures a high volume fraction of clasts mixing into the melt. Here, this complex debris flow is modeled using a simplified approach: when the temperature exceeds the solidus, (i) a pressure-dependent friction law (coefficient of 0.1–0.2 based on melt-lubricated faults [28]) is used at high strain rates (>10^{-4} s^{-1}) and (ii) a Newtonian fluid rheology is used at low strain rates (when the viscosity of the fluid dominates [29]).

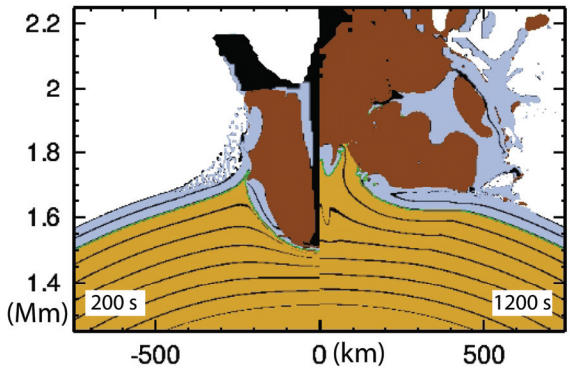

Figure 1. Snapshots of the transient cavity and maximum mantle uplift during Orientale-scale basin formation. Simulation of a 100-km diameter rocky projectile at 10.6 km/s onto 60-km thick crust with 0.5 Gyr thermal profile from [17] (2D, 2.5 km/cell). Colors denote composition (crust–blue; mantle–brown; projectile–dark brown; crust & mantle mixture–green) and lines denote stratigraphic deformation. Note the crust lining the transient cavity.

Impact Basin Formation Results. During collapse of the transient cavity, the strength of the melt-clast mixture inhibits significant overshoot of mantle material (Fig. 1). The final basin structure has two major features: (i) an inner basin filled with a mixture of melt and solid clasts and bounded by the cold folded crust and (ii) a shallow terrace of faulted and translated crust and mantle with an ejecta deposit (Fig. 2). The folded crust is a complex structure that experiences translation inward and then outward during collapse of the transient cavity. Using the updated mantle rheology, the melted mantle is largely confined to the inner basin. Discontinuous patches of melted mantle are emplaced on the basin terrace, and very finely dispersed mantle is ejected to greater distances. Similar results are found for all size basins.

Crustal material in the inner basin. The material within the inner basin is primarily of mantle origin as

most of the overlying original crust was excavated. However, the downward momentum of the projectile prevents excavation of all the crust; an area of crust comparable to the projectile cross section is trapped and lines the floor of the transient cavity (Fig. 1). Under expected impact velocities, the shock results in partial vaporization of crustal rocks [30]. The remaining liquid fraction is mixed with the molten mantle and will crystallize as new crust, on the order of a few km thick for lunar and martian basins, upon cooling of the basin. In addition, partial melting of the mantle may extract additional mass of crustal phases. At present, the numerical methods utilized in impact cratering models do not include the physics of phase separation between the gas and the liquid. In most cases, the boiling crustal phases are artificially treated as an intermediate density gas, which is removed from the basin floor via adiabatic expansion upon decompression.

Comparison to Observations. The simulation results reproduce the major features of impact basins: (1) Surface topography consisting of a flat-floored inner basin bounded by a gently sloped terrace to the crater rim. (2) The Moho topography agrees with geophysical inversion models [32]. The origin of the gravity anomaly may be explained by post-formation flexural adjustment [33]. (3) The inner basin will crystallize a layer of new crust. (4) The terrace zone contains discontinuous patches of ejected mantle. Olivine is detected spectroscopically in the terrace zones of impact basins on the Moon [4] and Mars [14, 15]. Based on these simulations, the olivine-bearing deposits are interpreted to be impact melts of mantle origin.

Conclusions. New insights into the multiphase flow of materials during impact basin formation reconcile the deep excavation into the mantle with limited distribution of mantle material on the surface. The olivine-rich deposits observed in the terrace zones of impact basins represent the most direct mantle samples available on planetary surfaces.

References. [1] Croft, S.K. (1980) *11th LPSC*, 2347-2378. [2] Williams, K.K. and M.T. Zuber (1998) *Icarus* **131**, 107-122. [3] Spudis, P.D. (1993) *The Geology of Multi-Ring Impact Basins*: Cambridge U.P. [4] Yamamoto, S., et al. (2010) *Nature Geosci.* **3**, 533-536. [5] Ivanov, B.A., et al. (2010) *Large Meteorite Impacts and Planetary Evolution IV*, GSA, p. 29-49. [6] Potter, R.W.K., et al. (2010) *LPSC* **41**, Abs. 1700. [7] Collins, G.S., et al. (2010) *Nördlingen Ries Crater Wkshp*, Abs. 7023. [8] Collins, G.S. and H.J. Melosh (2004) *LPSC* **35**, Abs. 1375. [9] Ivanov, B.A. (2007) *LPSC* **38**, Abs. 2003. [10] Hammond, N.P., et al. (2009) *LPSC* **40**, Abs. 1455. [11] Melosh, H.J. (1989) *Impact Cratering: A Geologic Process*. New York: Oxford U.P. [12] Billingham, L., et al. (2010) *LPSC* **41**, Abs. 1996. [13] Pierazzo E., N., et al. (2008) *MAPS* **43**, 1917-1938. [14] Poulet, F., et al. (2007) *JGR* **112**, E08S02. [15] Ody, A. and F. Poulet (2010) *LPSC* **42**. [16] McGlaun, J.M., et al. (1990) *Int. J. Impact Eng.* **10**, 351-360. [17] Spohn, T., et al. (2001) *Icarus* **149**, 54-65. [18] Hauck, S.A., II and R.J. Phillips (2002) *JGR* **107**, 5052. [19] Kerley, G.I. (1993), Report SAND93-0027, Sandia National Lab., p. 64. [20] Melosh, H.J. (2008), pers. comm. [21] Melosh, H.J. (2007) *MAPS* **42**, 2079-2098. [22] Senft, L.E. and S.T. Stewart (2009) *EPSL* **287**, 471-482. [23] Zucker, R.V. and S.T. Stewart (2010) *LPSC* **41**, Abs. 2722. [24] Kawazoe, T., et al. (2009) *PEPI* **174**, 128-137. [25] Zhang, J. and C. Herzberg (1994) *JGR* **99**, 17729-17742. [26] Croft, S.K. (1983) *JGR* **88**, B71-B89. [27] Iverson, R.M. (1997) *Rev. Geophys.* **35**, 245-296. [28] Del Gaudio, P., et al. (2009) *JGR* **114**, B06306. [29] Kohlstedt, D.L. (2002) *Rev. Min. Geochem.* **51**, 121-134. [30] Ahrens, T.J. and J.D. O'Keefe (1972) *Moon* **4**, 214-249. [31] Wieczorek, M.A. (2010), pers. comm. [32] Wieczorek, M.A. and R.J. Phillips (1999) *Icarus* **139**, 246-259. [33] Andrews-Hanna, J.C. and S.T. Stewart (2011) *LPSC* **42**, Abs. 2194.

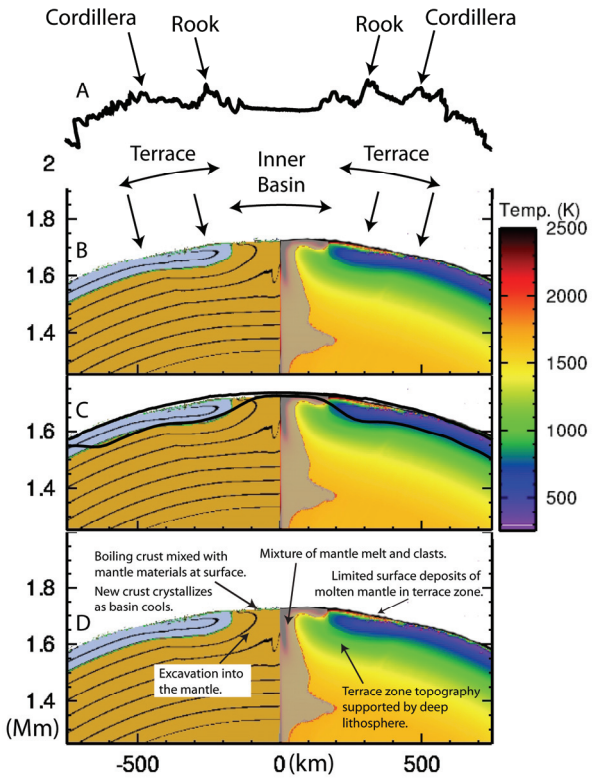

Figure 2. Final basin structure for Orientale scale impact event. A. LOLA N–S profile (vertically stretched). B. Temperatures (right) overlaid by grey zone are above the solidus will have gradient reduced by mixing in solid clasts (a process not modeled directly). Arrows denote features analogous to the Rook formation (hinge of the overturned cold crust) and the Cordillera ring (the outer edge of the terrace). C. Orientale surface and mantle topography to scale (crustal thickness model from [31]). D. Annotations.